Plasmonics
https://doi.org/10.1007/s11468-018-0713-7

Enhancing Diamond Fluorescence via Optimized Nanorod Dimer Configurations

András Szenes[1] · Balázs Bánhelyi[2] · Tibor Csendes[2] · Gábor Szabó[1] · Mária Csete[1]

Received: 24 September 2017 / Accepted: 13 February 2018

Abstract
Light extraction from silicon (SiV) and nitrogen (NV) vacancy diamond color centers coupled to plasmonic silver and gold nanorod dimers was numerically improved. Numerical optimization of the coupled dipolar emitter—plasmonic nanorod dimer configurations was realized to attain the highest possible fluorescence enhancement by simultaneously improving the color centers excitation and emission through antenna resonances. Conditional optimization was performed by setting a criterion regarding the minimum quantum efficiency of the coupled system (*cQE*) to minimize losses. By comparing restricted symmetric and allowed asymmetric dimers, the advantages of larger degrees of freedom achievable in asymmetric configurations was proven. The highest 2.59×10^8 fluorescence enhancement was achieved with 46.08% *cQE* via NV color center coupled to an asymmetric silver dimer. This is 3.17-times larger than the 8.19×10^7 enhancement in corresponding symmetric silver dimer configuration, which has larger 68.52% *cQE*. Among coupled SiV color centers the highest 1.04×10^8 fluorescence enhancement was achieved via asymmetric silver dimer with 37.83% *cQE*. This is 1.06-times larger than the 9.83×10^7 enhancement in corresponding symmetric silver dimer configuration, which has larger 57.46% *cQE*. Among gold nanorod coupled configurations the highest fluorescence enhancement of 4.75×10^4 was shown for SiV color center coupled to an asymmetric dimer with 21.8% *cQE*. The attained enhancement is 8.48- (92.42-) times larger than the 5.6×10^3 (5.14×10^2) fluorescence enhancement achievable via symmetric (asymmetric) gold nanorod dimer coupled to SiV (NV) color center, which is accompanied by 16.01% (7.66%) *cQE*.

Keywords Localized surface plasmon resonance · Nanorod dimer · Diamond vacancy center · Fluorescence enhancement · Numerical configuration optimization

Introduction

Improvement of photonic structures including single-photon emitters is crucial both in fundamental research and in various application areas of integrated photonic elements such as magnetic sensing and quantum information processing (QIP) [1–4]. Promising single-photon emitters for QIP applications are the nitrogen (NV) [5–7] and silicon (SiV) [8–11] vacancy diamond color centers due to their strong zero-phonon lines (ZPL) in the visible and in the near-infrared regions, respectively, which are accompanied by stable electron spin detectable even at room temperatures. SiV color centers are unique due to their narrow ZPL, which makes them particularly important for specific applications.

The phenomenon of well-known localized surface plasmon resonance (LSPR) occurs, when the light resonantly couples into the conductive electrons collective oscillation accompanied by volume charge accumulation in metal nanoparticles [12–14]. The E-field of localized plasmon modes is enhanced and confined inside regions significantly smaller than the excitation wavelength, which results in the modification of local density of states (LDOS) as well at the resonance frequency. As a result the fluorescent light emission can be enormously enhanced via plasmonic nanostructures, as it is proven by several examples in the literature [15–17]. To achieve the highest possible fluorescence enhancement the most efficient approach is the simultaneous improvement of the excitation

Electronic supplementary material The online version of this article (https://doi.org/10.1007/s11468-018-0713-7) contains supplementary material, which is available to authorized users.

✉ Mária Csete
mcsete@physx.u–szeged.hu

[1] Department of Optics and Quantum Electronics, University of Szeged, Dóm tér 9, Szeged 6720, Hungary

[2] Department of Computational Optimization, University of Szeged, Árpád tér 2, Szeged 6720, Hungary

Published online: 07 March 2018

and emission phenomenon [18, 19]. The emitter may couple the fluorescence light into the LSPR of a nearby metal particle, which can reradiate this energy with significantly improved efficiency and directivity due to its resonant antenna properties [19–24]. The enhancement of LDOS is much larger inside the nanogap between two plasmon resonant nanoparticles, e.g., noble metal spheres, ellipsoids, rods, tips, and cubes, than in the proximity of a single plasmonic nanoparticle [25–30]. Accordingly, the excitation rate of a diamond color center located in a dimer nanogap can be considerably enhanced. In addition to this, the hybridization of surface plasmons supported by the composing individual particles can also lead to various coupled modes depending on interaction geometry, which can promote larger fluorescence enhancement [29–32].

In a homogeneous environment the transition rate of NV color centers is in the interval of 1/12–1/22 ns^{-1} [5, 33], while the transition rate of SiV is in the order of 1/1 ns^{-1} [10, 33]. The decay rate of these color centers can be also improved in an inhomogeneous environment due to the Purcell effect [29, 34–39]. Moreover, spectral line-width narrowing [40] as well as resolution enhancement in microscopy [41, 42] can be achieved.

The importance of optimal emitter-plasmonic nanoantenna coupling configuration has already been recognized in previous studies [24, 27, 30, 38]. However, most of the experimental works on diamond demonstrate only moderate color center fluorescence improvement caused by the mismatch of the scattering cross-section peak of the nanoparticle systems and the ZPL [29]. The concept of our present study is that to fully exploit the capabilities of LSPR on noble metal nanoparticle dimers in diamond color center fluorescence improvement, adjoint geometry, and illumination direction optimization is required. Accordingly, in this paper the nanorod dimer configurations, i.e., geometrical parameters and illumination conditions are numerically optimized to enhance the fluorescence of NV and SiV diamond color centers.

Methods

To realize conditional coupled emitter—plasmonic nanoparticle configuration optimization, a special numerical methodology was developed based on the radio frequency module of the commercially available COMSOL Multiphysics software. The conditional optimization methodology and the implementation of the GLOBAL optimization algorithm is described in our previous works [38, 43, 44]. Similarly to the optimization of single color center—single nanorod coupled systems [38], the color centers were modeled as pure electric point dipoles embedded into a bulk diamond dielectric medium, but in present study, this medium surrounds not a singlet but a dimer of metal nanorods, and both of them is composed of two semispheres connected by a cylinder. To study the near-field phenomena and the far-field optical response of the single color center coupled to the noble metal nanorod dimer, scattering boundary condition was applied and the model was enclosed by a spherical PML layer. The minimum mesh size of 0.3 nm was applied inside a tiny bag, which was artificially created to read out the dipole response.

The effect of dimer coupling on the optical response of the color center is traditionally characterized via the emitter's *Purcell factor*, which in case of the special coupled system is the ratio of dipole powers emitted in presence of the nanorod dimer (P^{total}) and in vacuum ($P_0{}^{\text{radiative}}$) [29–35]:

$$\text{Purcell factor} = \frac{\text{P}^{\text{total}}}{\text{P}_0^{\text{radiative}}} = \frac{\text{P}^{\text{radiative}} + \text{P}^{\text{non-radiative}}}{\text{P}_0^{\text{radiative}}}. \quad (1)$$

The coupled color center—nanorod dimer system's radiative rate enhancement (δR) is specified as the power radiated into the far-field ($P^{\text{radiative}}$) in presence of nanorod dimer divided by the dipole power emitted in vacuum:

$$\delta R = \frac{P^{\text{radiative}}}{P_0{}^{\text{radiative}}}, \quad (2)$$

and the coupled color center—nanorod dimer system's quantum efficiency (QE) is the ratio of the δR radiative rate enhancement (Eq. (2) and of the *Purcell factor* (Eq. (1):

$$\text{QE} = \frac{\delta\text{R}}{\text{Purcell factor}}. \quad (3)$$

The value of QE was corrected by taking into account the intrinsic 10 and 90% QE_0 of SiV and NV color centers during a post-processing in order to determine the cQE corrected quantum efficiency of the coupled color centers:

$$\text{cQE} = \frac{\delta\text{R}}{\text{Purcell factor} + \frac{1\text{-QE}_0}{\text{QE}_0}}. \quad (4)$$

According to reciprocity theorem, the excitation enhancement can be treated as the emission enhancement, namely the analogous *Purcell factor*, δR, and QE quantities describe the system of a dipolar color center coupled to metal nanorod dimer but emitting at the wavelength of excitation. The emission was qualified by the transition rate modification and the improved directivity as well (Tables S1-S3) [19, 24, 45, 46].

The selected objective function of the numerical optimization was the product of δR radiative rate enhancements at the excitation and emission wavelengths, since this so-called P_x *factor* describes the complete color center fluorescence enhancement. In many QIP applications, high QE quantum efficiency of the coupled systems is essential; hence, multi-step conditional optimizations were realized to achieve the highest P_x *factor* by setting gradually increasing criteria regarding the minimum cQE corrected quantum efficiency that has to be

reached at the emission wavelength. Dimers made both of gold and silver were studied, by defining their dielectric properties inside the noble metal nanorods. The geometrical parameters that were varied during numerical optimization include the nanorod short and long axis, which were tuned in [13–158 nm] and in an offset [15–160 nm] intervals, respectively, while the nanorod dimer nanogap was varied in [4–20 nm] interval. While simulating NV coupling the dipolar emitter deposited into the center of the dimer gap had a transition dipole moment parallel to the axis defined by the long axes of nanorods. In contrast, while simulating SiV coupling the two dipoles corresponding to excitation and emission were rotated to +/− 45° with respect to the dimer axis according to their perpendicularity, to ensure balanced contribution of the excitation and emission enhancement phenomena to the fluorescence improvement qualified by the P_x *factor* [9, 10].

Results

First the symmetry of the components in nanorod dimers was demanded then the optimization was repeated by allowing different geometrical parameters for the nanorod components in asymmetric dimers. To determine the optical response, the complete δR radiative rate enhancement spectra were determined between 500 and 800 nm. Then the surface charge and near-field distribution, as well as the far-field radiation pattern [20, 23], namely the angular distribution of the emitted power, was inspected at the excitation and emission wavelengths to reveal the underlying nanophotonics. In the main text, the optimized configurations corresponding to the highest achievable P_x *factor* are presented regardless the accompanying *cQE*. Data on the geometrical properties and optical responses of these optimized systems (Online Resource, Tables S1-S3), the transition rate and directivity achieved via the optimized configurations exhibiting the highest P_x *factor*, as well as further information on configurations determined by optimization with different *cQE* criteria are provided in a Supplementary Material (Online Resource, Figs. S1-S4, Tables S1-S3).

SiV Color Center Coupled to Symmetric Nanorod Dimers

In the optimized configuration of SiV color center coupled to symmetric silver nanorod dimers, the components are elongated (Online Resource, Table S1). On the *Purcell* (*QE*) spectrum a local maximum is slightly detuned from the excitation wavelength, while the global maximum coincides with (is detuned above) the emission wavelength (Fig. 1a).

Both the excitation and emission phenomena are significantly enhanced; however, the local maximum in δR radiative rate is slightly more detuned from the excitation, than from the emission wavelength. The achieved 3.36×10^3 and 2.93×10^4 δR radiative rate enhancements with 7.2 and − 3.6 nm detuning at the excitation and emission wavelength result in 9.83×10^7 P_x *factor*, and the coupled color center exhibits 57.46% *cQE*.

At the excitation wavelength the $2 \times \lambda/2$ type volume charge distribution on both composing silver nanorods is accompanied by a strong parallel surface dipole, while at the emission wavelength a more commensurate parallel surface dipole accompanies the $1 \times \lambda/2$ antenna resonances (Fig. 1b, c). The dipolar emitter corresponding to SiV center is efficiently coupled both at the excitation and emission wavelength according to the regular dipolar far-field pattern perpendicular to the dimer axes (Fig. 1d). The SiV fluorescence is enhanced via coupling to second and first order antenna modes on the silver nanorods in the symmetric dimer at the excitation and emission wavelength, respectively. The transition rate is enhanced up to 1/0.2 ps^{-1}, the achieved directivity is 7.21 at the emission, and the emission occurs perpendicularly to the dimer axis (Fig. 1 and S1).

The optimization of symmetric gold nanorod dimers with the same criteria resulted in a coupled color center—dimer configuration consisting of slightly less elongated

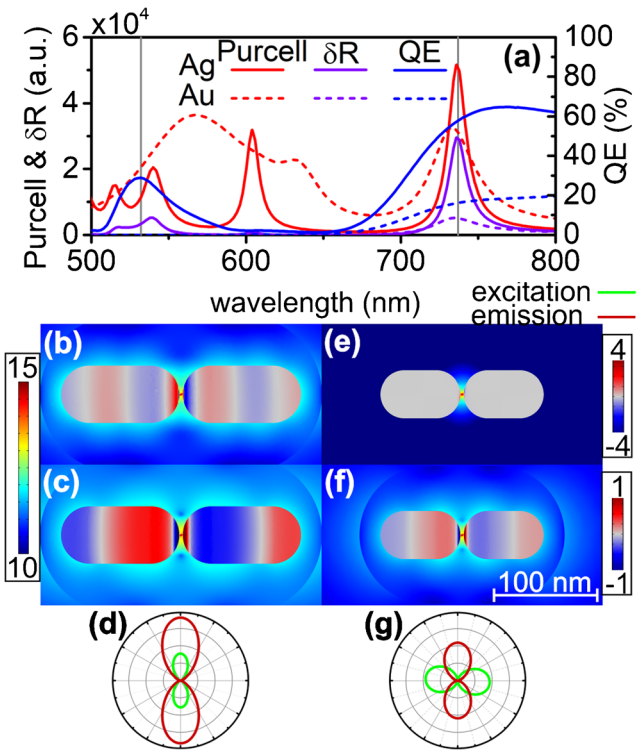

Fig. 1 Optical response of a SiV color center coupled to symmetric nanorod dimer. **a** *Purcell factor*, quantum efficiency (*QE*) and radiative rate enhancement (δR) spectra. **b**, **c**, **e**, **f** Surface charge and near-field distribution on a logarithmic scale in arbitrary units, **b**, **e** at excitation and **c**, **f** at emission **d**, **g** far-field radiation pattern; **b**, **c**, **d** silver and **e**, **f**, **g** gold dimer (in **g** the power at excitation (emission) is multiplied by 4 (4000) to improve visibility)

components (Online Resource, Table S1). On the *Purcell* spectrum the global maximum is well above the excitation wavelength, while a local maximum almost coincides with the emission wavelength (Fig. 1a). The *QE* quantum efficiency is relatively low at the excitation, but gradually increases towards the emission wavelength.

On the δR spectrum one single peak is noticeable, which is tuned to the emission wavelength. The achieved 1.12 and 5.00×10^3 δR radiative rate enhancements with 72.2 and −3.6 nm detuning at the excitation and emission wavelength result in 5.60×10^3 P_x *factor*, and the coupled color center exhibits 16.01% *cQE*.

At the excitation wavelength the symmetric nanorod dimer does not show a coupled resonance, since at the nanogap only a weak localized surface dipole is recognizable (Fig. 1e). Accordingly, a weak near-field enhancement is recognizable around the nanorods and an anomalous dipolar far-field pattern aligned along the dimer axis is observable (Fig. 1g). At the emission wavelength on both composing gold nanorods, $1 \times \lambda/2$ dipolar volume resonance appears, which is accompanied by a parallel localized surface dipole (Fig. 1f). The efficient emitter—dimer coupling results in a regular dipolar far-field pattern perpendicularly to the dimer axis (Fig. 1g). The SiV emission is enhanced via coupling to first order antenna modes on the gold nanorods in the symmetric dimer. The transition rate is enhanced to 1/0.32 ps^{-1}, the achieved directivity is 6.35, and the emission occurs perpendicularly to the dimer axis (Fig. 1 and S1).

Comparison of the symmetric silver and gold nanorod dimer coupled SiV systems shows that via silver the radiative rate enhancement is 1.76×10^4-times better, with 10-times smaller (the same) detuning at the excitation (emission) wavelength.

SiV Color Center Coupled to Asymmetric Nanorod Dimers

When different geometrical parameters are allowed for the components of the nanorod dimer, the optimization procedure results in a strongly asymmetric silver nanorod dimer configuration (Online Resource, Table S2). On the *Purcell factor* (*QE*) spectrum a local maximum appears, which is close to (coincides with) the excitation wavelength, while the emission wavelength almost coincides again with one of the (is far from two neighboring) resonance peaks (Fig. 2a). The δR radiative rate enhancement spectrum shows that the excitation and emission phenomenon is significantly enhanced via resonance, which results in a local and global maximum, respectively. The achieved 3.00×10^3 and 3.47×10^4 δR radiative rate enhancements with 0.0 and 0.8 nm detuning at the excitation and emission wavelength result in 1.04×10^8 P_x *factor*, and the coupled emitter exhibits 37.83% *cQE*.

At the excitation wavelength, a charge distribution corresponding to $2 \times \lambda/2$ ($1 \times \lambda/2$) volume resonance appears on the larger (smaller) silver nanorod, which is locally enhanced by a parallel surface dipole at the dimer nanogap (Fig. 2b). At the emission wavelength, a charge distribution corresponding to an antiparallel $1 \times \lambda/2$ volume resonance is observable on both silver nanorods with a reversing localized surface dipole at the dimer nanogap (Fig. 2c). According to the efficiently coupled emitter-dimer, regular dipolar far-field pattern is observable at both wavelengths perpendicularly to the silver nanorod dimer axis, which has a strongly and slightly asymmetrical scattering distribution at excitation (emission) wavelength (Fig. 2d). In case of the asymmetric silver dimer, the SiV fluorescence is enhanced via coupling to co-existent second and first order antenna modes on the large and small nanorod at the excitation wavelength and to first order antenna modes on both nanorods at the emission wavelength. The rate is enhanced up to 1/0.11 ps^{-1}, the achieved directivity is 5.1, and the emission occurs at 64.8° with respect to the dimer axes, namely slightly towards the smaller nanorod (Fig. 2 and S2).

The gold nanorod dimer optimization performed by allowing different geometrical parameters for the components resulted in a strongly asymmetric configuration (Online

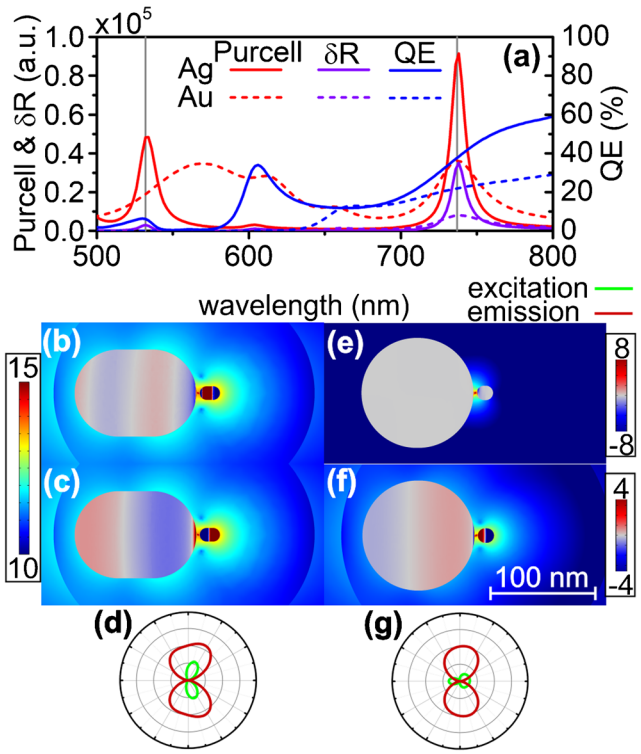

Fig. 2 Optical response of a SiV color center coupled to asymmetric nanorod dimer. **a** *Purcell factor*, quantum efficiency (*QE*), and radiative rate enhancement (δR) spectra. **b**, **e**, **c**, **f** Surface charge and near-field distribution on a logarithmic scale in arbitrary units, **b**, **e** at excitation and **c**, **f** at emission, **d**, **g** far-field radiation pattern; **b**, **c**, **d** silver and **e**, **f**, **g** gold dimer (in **g** the power at excitation (emission) is multiplied by 4 (400) to improve visibility)

Resource, Table S2). On the *Purcell factor* spectrum one broad local resonance is detuned above the excitation wavelength, while the narrower global maximum almost coincides with the emission wavelength (Fig. 2a). No local maximum is observable on the *QE* spectrum at the excitation wavelength and the emission is on the side of a broad global *QE* maximum. On the δR radiative rate enhancement spectrum, a local maximum appears far from the excitation wavelength; however, the global maximum is tuned close to the emission wavelength. The achieved 5.97 and 7.95×10^3 δR radiative rate enhancements with − 5.2 and 0.6 nm detuning at the excitation and emission wavelength result in 4.75×10^4 P_x *factor*, and the coupled color center exhibits 21.80% *cQE*.

At the excitation wavelength, a weak surface dipole appears at the dimer nanogap, while no significant near-field enhancement arises on either of the gold nanorods, which indicates an off-resonant configuration (Fig. 2e). Accordingly, the anomalous far-field pattern, which is aligned along the dimer axis, is determined only by the uncoupled emitter and indicates an asymmetrical scattering distribution defined by the asymmetry of the gold nanorod dimer (Fig. 2g). At emission wavelength both nanorods exhibit strong resonance in $1 \times \lambda/2$ volume mode. Furthermore, a reversal dipolar charge distribution develops on the coupled nanorods, in addition to this a localized surface dipole is also observable at the dimer nanogap, which is parallel to that on the larger nanorod (Fig. 2f). The regular dipolar far-field radiation pattern corresponds to an efficiently coupled system, which emits throughout a wide polar angle region. The SiV emission is enhanced via coupling to first order antenna modes on both nanorods in the asymmetric gold dimer. The transition rate is enhanced up to 1/0.27 ps^{-1}, the achieved 5.1 directivity equals to that of the asymmetric silver nanorod dimer, and the emission occurs at 79.2°, again slightly towards to the smaller nanorod (Fig. 2 and S2). Comparison of the asymmetric silver and gold nanorod dimer coupled SiV systems shows that 2.19×10^3-times better radiative rate enhancement is achievable via silver, with amended (1.33-times larger) detuning at the excitation (emission) wavelength.

NV Color Center Coupled to Symmetric Nanorod Dimers

When the fluorescence of NV color center coupled to symmetric silver dimer is improved, the optimized configuration consists of sphere-like nanorods (Online Resource, Table S1). On the *Purcell factor* spectrum, a narrow coincident resonance peak is observable at the excitation wavelength, while the side of a broader resonance peak enhances the emission phenomenon (Fig. 3a). The excitation is on the side of a high *QE* resonance, while the emission wavelength is in between a broad local and the global *QE* maximum.

On the δR radiative rate enhancement spectrum, a local maximum is tuned to (strongly detuned from) the excitation

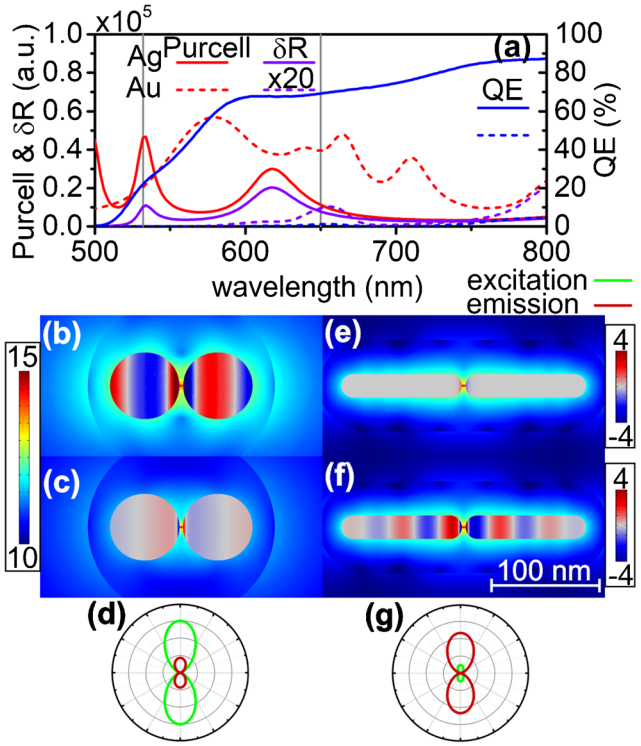

Fig. 3 Optical response of an NV color center coupled to symmetric nanorod dimer. **a** *Purcell factor*, quantum efficiency (*QE*), and radiative rate enhancement (δR) spectra. **b**, **c**, **e**, **f** Surface charge and near-field distribution on a logarithmic scale in arbitrary units, **b**, **c** at excitation and **e**, **f** at emission, **d**, **g** far-field radiation pattern; **b**, **c**, **d** silver and **e**, **f**, **g** gold nanorod dimer (in **a** the Au excitation signal is multiplied by 20 and in **g** the power at excitation (emission) is multiplied by 40 (4000) to improve visibility)

(emission) wavelength. The achieved 1.06×10^4 and 7.70×10^3 δR radiative rate enhancements with 1.8 and − 32.2 nm detuning at the excitation and emission wavelength result in 8.19×10^7 P_x *factor*, and the coupled color center exhibits 68.52% *cQE*.

The excitation phenomenon is enhanced via strong $1 \times \lambda/2$ antiparallel antenna resonances on both composing nanorods, which volume resonances are accompanied by a strong and confined reversing surface dipole at the dimer nanogap (Fig. 3b). The emission phenomenon is enhanced via a weak $1 \times \lambda/2$ resonance, parallel volume resonance appears on both composing nanorods, which is accompanied by a relatively stronger parallel surface dipole at the dimer nanogap (Fig. 3c). The uniquely stronger excitation enhancement is indicated by the larger lobes of the regular dipolar far-field pattern; however, the emission occurs into a relatively broader polar angle region through a regular dipolar far-field pattern (Fig. 3d). The NV fluorescence is enhanced via strong and weak coupling to first order antenna modes on the nanorods in the symmetric silver dimer at the excitation and emission wavelength, respectively. The transition rate is enhanced up to 1/2.18 ps^{-1}, the achieved directivity is 6.04, and the

emission occurs perpendicularly to the dimer axis (Fig. 3 and S3). Symmetric silver nanorod dimer coupling makes it possible to attain 0.83-times smaller P_x *factor* for NV than for SiV color center with 4-times smaller and 8.94-times larger detuning at the excitation and emission wavelength, respectively.

The optimization of the symmetric gold nanorod dimer with the same criteria resulted in a strongly elongated nanoantennas compared to all previous optimized configurations (Online Resource, Table S1). The *Purcell factor* spectrum indicates that the excitation wavelength is well before the global resonance maximum, the emission is in between two local resonance maxima, while only a small local *QE* maximum appears at the emission wavelength (Fig. 3a).

The emission phenomenon is enhanced more significantly; however, the global maximum on the δR radiative rate enhancement spectrum is at a noticeably larger wavelength, than the NV emission. The resulted 0.45 and 4.75×10^2 δR radiative rate enhancements with 83 and 6.8 nm detuning at the excitation and emission wavelength result in 2.14×10^2 P_x *factor*, and the coupled color center exhibits very low 1.19% *cQE*.

The excitation phenomenon is enhanced by a weak surface dipole at the nanogap of the nanorod dimer (Fig. 3e). There is no significant near-field enhancement on either of the gold nanorods. According to the weakly coupled emitter-dimer configuration the far-field radiation is also weak; however, it exhibits a regular dipolar characteristics (Fig. 3g). The emission phenomenon is enhanced via a $3 \times \lambda/2$ antenna resonance on both composing gold nanorods, in addition to these volume resonances the E-field is strongly enhanced around the interfacial segments by the surface dipole at the dimer nanogap (Fig. 3f). Accordingly, the resonance is accompanied by a much stronger near-field enhancement around the gold nanorods and by a regular dipolar far-field radiation pattern perpendicular to the dimer axis, which indicates a much stronger enhancement than at the excitation. The NV emission is enhanced via coupling to third order antenna modes on the composing nanorods in the symmetric gold dimer. The transition rate is enhanced to 1/0.61 ps^{-1}, the achieved directivity is 6.63, and the emission occurs again perpendicularly to the dimer axis (Fig. 3 and S3). Symmetric gold nanorod dimer coupling allows to attain 0.04-times smaller P_x *factor* for NV, than for SiV with 1.15- and 1.89-times larger detuning at the excitation and emission wavelength, respectively.

Comparison of the symmetric silver and gold nanorod dimer coupled NV systems shows that via silver the fluorescence enhancement is 3.83×10^5-times better and 46.11-times smaller (4.74-times larger) detuning is achievable at the excitation (emission) wavelength.

NV Color Center Coupled to Asymmetric Nanorod Dimers

The optimization performed by allowing different geometrical parameters for the components of a silver dimer coupled to NV center systems resulted in a strongly asymmetric nanorod dimer configuration (Online Resource, Table S2). Local *Purcell factor* (*QE*) resonance peak is tuned to (detuned from) the excitation and coincides with emission wavelength (Fig. 4a).

The δR radiative rate spectrum indicates that the excitation and emission phenomenon is enhanced simultaneously. A local (the global) maximum on the δR radiative rate spectrum coincides with the excitation (emission) wavelength. The achieved 9.00×10^3 and 2.88×10^4 δR radiative rate enhancements with 1 and − 0.4 nm detuning at the excitation and emission wavelength result in 2.59×10^8 P_x *factor*, and the coupled color center exhibits 46.08% *cQE*.

On the optimized asymmetric silver nanorod dimer, the charge distribution at the excitation wavelength exhibits $2 \times \lambda/2$ quadrupolar volume—parallel dipolar surface—$1 \times \lambda/2$ dipolar volume modes, which are accompanied by a quadrupolar far-field radiation pattern (Fig. 4b,

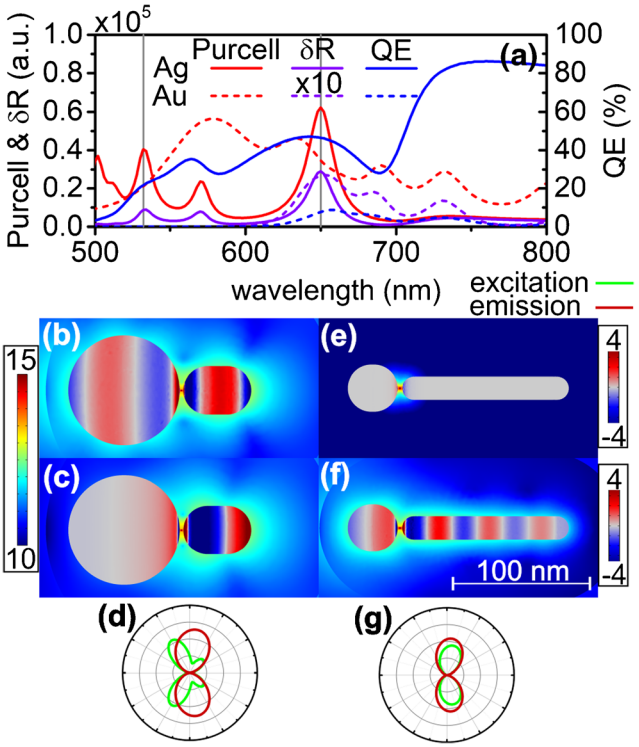

Fig. 4 Optical response of an NV color center coupled to asymmetric nanorod dimer. **a** *Purcell factor*, quantum efficiency (*QE*) and radiative rate enhancement (δR) spectra. **b**, **c**, **e**, **f** Surface charge and near-field distribution on a logarithmic scale in arbitrary units, **b**, **e** at excitation and **c**, **f** at emission, **d**, **g** far-field radiation pattern, **b**, **c**, **d** silver **e**, **f**, **g** gold nanorod dimer (in **a** signal of Au at excitation is multiplied by 10 and in **g** the power is multiplied by 8 and 40,000 to improve visibility)

d). The charge distribution at the emission exhibits $1 \times \lambda/2$ dipolar volume—parallel dipolar surface—$1 \times \lambda/2$ dipolar volume modes, while also the near-field shows that only the smaller silver nanorod is strongly resonant (Fig. 4c). The regular dipolar far-field radiation pattern perpendicularly to the dimer axis indicates efficient emitter-dimer coupling. The NV fluorescence is enhanced via coupling to co-existent second and first order modes on the larger and smaller nanorod at the excitation wavelength and via first order antenna modes at the emission wavelength in case of the asymmetric silver dimer. The transition rate is enhanced to 1/0.39 ps^{-1}, the achieved directivity is 5.63, and the emission occurs at 79.2° with respect to the dimer axis, i.e., slightly towards the smaller nanorod of the asymmetric silver dimer (Fig. 3 and S3). Asymmetric silver nanorod dimer coupling makes it possible to achieve 2.49-times larger P_x *factor* for NV, than for SiV with 10-times larger and 2-times smaller detuning at the excitation and emission wavelength, respectively.

The optimization performed by allowing different geometrical parameters for the components resulted in a strongly asymmetric gold nanorod dimer configuration (Online Resource, Table S2). Based on the *Purcell factor* spectrum neither the excitation nor the emission wavelength is coincident with a resonance (Fig. 4a). No local *QE* maximum appears at the excitation wavelength; however, the global *QE* maximum is almost perfectly tuned to the emission wavelength.

Accordingly, no resonance peaks appear on the δR spectra around the excitation and significant enhancement is observable only at the emission wavelength. The achieved 0.19 and 2.68×10^3 δR radiative rate enhancements with 118.8 and 1.8 nm detuning at the excitation and emission wavelength result in 5.14×10^2 P_x *factor*, and the coupled color center exhibits 7.66% *cQE*.

At the wavelength of excitation only a surface dipole is observable at the nanogap of the asymmetric gold dimer (Fig. 4e). No significant near-field enhancement occurs, the regular dipolar far-field radiation pattern is determined by the coupled emitter with a slightly asymmetrical scattering distribution defined by the spherical nanoparticle (Fig. 4g). At the emission wavelength on the spherical nanorod $1 \times \lambda/2$ dipolar volume—inside the gap parallel dipolar surface—on the more elongated nanorod $3 \times \lambda/2$ volume mode is accompanied by a regular dipolar far-field radiation pattern perpendicular to the dimer axis (Fig. 4f). The NV emission is enhanced via coupling to co-existent first and third order antenna modes on the smaller and larger nanorod in the asymmetric gold dimer, respectively. The transition rate is enhanced up to 1/0.7 ps^{-1}, the achieved directivity is 6.38, and the emission occurs at 82.8°, namely slightly towards the nanorod having a smaller (larger) short (long) axis (Fig. 4 and S4). Asymmetric gold nanorod dimer coupling allows 0.01-times smaller P_x *factor* for NV, than for SiV with 22.85- and 3 times-larger detuning at the excitation and emission wavelength, respectively.

Comparison of the asymmetric silver and gold nanorod dimer coupled NV systems shows that via silver the fluorescence enhancement is 5.05×10^5-times better; however, 118.8- (4.5-) times smaller detuning is achievable at the excitation (emission).

Conclusion

In conclusion, the restricted symmetric configuration of the optimized nanorod dimers predetermines the symmetry of the charge, near-field and resistive heating distribution on the components. In the allowed asymmetric configurations, the simultaneous excitation and emission enhancement is more significant than in symmetric configurations due to the larger number of independently tunable nanorod parameters. Co-existent antenna modes can be at play in all asymmetric dimers, these appear at the excitation wavelength in asymmetric silver dimer coupled SiV and NV systems, while in case of asymmetric gold dimer coupled NV system, different modes co-exist at the emission wavelength. The asymmetric gold dimer coupled to SiV is the exception, where only uniform modes appear at the emission wavelength. No resonant modes appear in any gold dimer coupled color center systems at the excitation wavelength. Accordingly, both the achieved P_x *factor* and the *cQE* corrected quantum efficiency is higher in case of silver nanorod dimers than those achievable via coupling to gold dimers in all inspected coupled systems. The highest fluorescence enhancement among the inspected systems is 2.59×10^8 with 46.08% *cQE*, which is achievable via NV color center coupled to an asymmetric silver nanorod dimer. The highest 1.04×10^8 SiV enhancement is achieved via coupling to an asymmetric silver nanorod dimer with 37.83% *cQE*. Based on these results, asymmetric silver dimers are proposed for enhancing both of the SiV and NV color centers. Among gold nanorod dimers the highest 4.75×10^4 P_x *factor* along with 21.8% *cQE* is observable, when SiV color center is coupled to asymmetric dimer antennas. If the chemically inert gold is preferred, then asymmetric dimers of gold nanorods are proposed to enhance the fluorescence. Apart from asymmetric silver nanorod dimers SiV proved to be better regarding the achievable fluorescence enhancement. SiV color center coupled to gold nanorod dimers show one (two) orders of magnitude larger fluorescence enhancement, than the NV coupled to gold nanorod dimers, in symmetric (asymmetric) configurations.

See supplementary material for detailed information about the presented configurations as well as data of conditionally optimized nanorod dimer systems.

Acknowledgements Mária Csete acknowledges that the project was supported by the János Bolyai Research Scholarship of the Hungarian Academy of Sciences. The authors would like to thank Dávid Vass and Géza Veszprémi for figure preparation.

Funding information The research was supported by National Research, Development and Innovation Office-NKFIH through project "Optimized nanoplasmonics" K116362.

References

1. Maze JR, Stanwix PL, Hodges JS, Hong S, Taylor JM, Cappellaro P, Jiang L, Gurudev Dutt MV, Togan E, Zibrov AS, Yacoby A, Walsworth RL, Lukin MD (2008) Nanoscale magnetic sensing with an individual electronic spin in diamond. Nature 455:644–647
2. Benjamin SC, Lovett BW, Smith JM (2009) Prospects for measurement-based quantum computing with solid state spins. Laser Photonics Rev 3:556–574
3. Aharonovich I, Greentree AD, Prawer S (2011) Diamond photonics. Nat Photonics 5:397–405
4. Bernien H, Hensen B, Pfaff W, Koolstra G, Blok MS, Robledo L, Taminiau TH, Markham M, Twitchen DJ, Childress L, Hanson R (2013) Heralded entanglement between solid-state qubits separated by three metres. Nature 497:86–90
5. Manson NB, Harrison JP, Sellars MJ (2006) Nitrogen-vacancy center in diamond: model of the electronic structure and associated dynamics. Phys Rev B 74:104303
6. Maze JR, Gali A, Togan E, Chu Y, Trifonov A, Kaxiras E, Lukin MD (2011) Properties of nitrogen-vacancy centers in diamond: the group theoretic approach. New J Phys 13:025025
7. Bayat K, Choy J, Baroughi MF, Meesala S, Loncar M Efficient, uniform, and large area microwave magnetic coupling to NV centers in diamond using double split-ring resonators. Nano Lett 14: 1208–1213
8. Gali A, Maze JR (2013) Ab initio study of the split silicon-vacancy defect in diamond: electronic structure and related properties. Phys Rev B 88:235205
9. Rogers LJ, Jahnke KD, Doherty MW, Dietrich A, McGuinness LP, Müller C, Teraji T, Sumiya H, Isoya J, Manson NB, Jelezko F (2014) Electronic structure of the negatively charged silicon-vacancy center in diamond. Phys Rev B 89:235101
10. Rogers LJ, Jahnke KD, Teraji T, Marseglia L, Müller C, Naydenov B, Schauffert H, Kranz C, Isoya J, McGuinness LP, Jelezko F (2014) Multiple intrinsically identical single-photon emitters in the solid state. Nat Commun 5:4739
11. Vlasov II, Shiryaev AA, Rendler T, Steinert S, Lee SY, Antonov D, Vörös M, Jelezko F, Fisenko AV, Semjonova LF, Biskupek J, Kaiser U, Lebedev OI, Sildos I, Hemmer PR, Konov VI, Gali A, Wrachtrupm (2014) Molecular-sized fluorescent nanodiamonds. J Nat Nanotechnol 9:54–58
12. Davis TJ, Gómez DE (2017) Colloquium: an algebraic model of localized surface plasmons and their interactions. Rev Mod Phys 89:011003
13. Link S, El-Sayed MA (1999) Spectral properties and relaxation dynamics of surface plasmon electronic oscillations in gold and silver nanodots and nanorods. J Phys Chem B 103:8410–8426
14. Cao J, Sun T, Grattan KTV (2014) Gold nanorod-based localized surface plasmon resonance biosensors: a review. Sensor Actuat B Chem 195:332–351
15. Moskovits M (1985) Surface-enhanced spectroscopy. Rev Mod Phys 57:783–828
16. Pelton M (2015) Modified spontaneous emission in nanophotonic structures. Nat Photonics 9:427–435
17. Yang Y, Zhen B, Hsu CW, Miller OD, Joannopoulos JD, Soljačić M (2016) Optically thin metallic films for high-radiative-efficiency plasmonics. Nano Lett 16:4110–4117
18. Tame MS, McEnery KR, Özdemir SK, Lee J, Maier SA, Kim MS (2013) Quantum plasmonics. Nat Phys 9:329–340
19. Taminiau TH, Stefani FD, van Hulst NF (2008) Enhanced directional excitation and emission of single emitters by a nano-optical Yagi-Uda antenna. Opt Express 16(14):10858–10866
20. Taminiau TH, Stefani FD, van Hulst NF (2008) Single emitters coupled to plasmonic nano-antennas: angular emission and collection efficiency. New J Phys 10:105005
21. Hoang TB, Akselrod GM, Argyropoulos C, Huang J, Smith DR, Mikkelsen MH (2015) Ultrafast spontaneous emission source using plasmonic nanoantennas. Nat Commun 6:7788
22. Dorfmüller J, Vogelgesang R, Khunsin W, Rockstuhl C, Etrich C, Kern K (2010) Plasmonic nanowire antennas: experiment, simulation, and theory. Nano Lett 10:3596–3603
23. Hancu IM, Curto AG, Castro-Lopez M, Kuttge M, van Hulst NF (2014) Multipolar interference for directed light emission. Nano Lett 14:166–171
24. Mahmoud KR, Hussein M, Hameed MFO, Obayya SSA (2017) Super directive Yagi–Uda nanoantennas with an ellipsoid reflector for optimal radiation emission. J Opt Soc Am B 34(10):2041–2049
25. Muskens OL, Giannini V, Sánchez-Gil JA, Gómez Rivas J (2007) Strong enhancement of the radiative decay rate of emitters by single plasmonic nanoantennas. Nano Lett 7:2871–2875
26. Rogobete L, Kaminski F, Agio M, Sandoghdar V (2007) Design of plasmonic nanoantennae for enhancing spontaneous emission. Opt Lett 32:1623–1625
27. Toroghi S, Kik PG (2012) Cascaded field enhancement in plasmon resonant dimer nanoantennas compatible with two-dimensional nanofabrication methods. Appl Phys Lett 101:013116
28. Duan H, Fernández-Domínguez AI, Bosman M, Maier SA, Yang JKW (2012) Nanoplasmonics: classical down to the nanometer scale. Nano Lett 12:1683–1689
29. Andersen SKH, Khumar S, Bozhevolnyi SI (2017) Ultrabright linearly polarized photon generation from a nitrogen vacancy center in a nanocube dimer antenna. Nano Lett 17:3889–3895
30. El-Toukhy YM, Hussein M, Hameed MFO, Obayya SSA. (2017) Plasmonics 1-8
31. Funston AM, Novo C, Davis TJ, Mulvaney P (2009) Plasmon coupling of gold nanorods at short distances and in different geometries. Nano Lett 9:1651–1658
32. Abb M, Wang Y, Albella P, de Groot CH, Aizpurua J, Muskens OL (2012) Interference, coupling, and nonlinear control of high-order modes in single asymmetric nanoantennas. ACS Nano 6:6462–6470
33. Aharonovich I, Englund D, Toth M (2016) Solid-state single-photon emitters. Nat Photonics 10:631–641
34. Choy JT, Hausmann BJM, Babinec TM, Bulu I, Khan M, Maletinsky P, Yacoby A, Lončar M (2011) Enhanced single-photon emission from a diamond–silver aperture. Nat Photonics 5:738–743
35. de Leon NP, Shields BJ, Yu CL, Englund DE, Akimov AV, Lukin MD, Park H (2012) Tailoring light-matter interaction with a nanoscale plasmon resonator. Phys Rev Lett 108:226803
36. Kolesov R, Grotz B, Balasubramanian G, RStöhr RJ, Nicolet AAL, Hemmer PR, Jelezko F, Wrachtrup J (2009) Wave–particle duality of single surface plasmon polaritons. Nat Phys 5:470–474
37. Wolf SA, Rosenberg I, Rapaport R, Bar-Gill N (2015) Purcell-enhanced optical spin readout of nitrogen-vacancy centers in diamond. Phys Rev B 92:235410

38. Szenes A, Bánhelyi B, Szabó LZ, Szabó G, Csendes T, Csete M (2017) Enhancing diamond color center fluorescence via optimized plasmonic nanorod configuration. Plasmonics 12:1263–1280
39. Kumar S, Huck A, Chen Y, Andersen UL (2013) Coupling of a single quantum emitter to end-to-end aligned silver nanowires. Appl Phys Lett 102:103106
40. Cheng S, Song J, Wang Q, Liu J, Li H, Zhang B (2015) Plasmon resonance enhanced temperature-dependent photoluminescence of Si-V centers in diamond. Appl Phys Lett 107:211905
41. Schell AW, Kewes G, Hanke T, Leitenstorfer A, Bratschitsch R, Benson O, Aichele T (2011) Single defect centers in diamond nanocrystals as quantum probes for plasmonic nanostructures. Opt Express 19:79147920
42. Hui YY, Lu YC, Su LJ, Fang CY, Hsu JH, Chang HC (2013) Tip-enhanced sub-diffraction fluorescence imaging of nitrogen-vacancy centers in nanodiamonds. Appl Phys Lett 102_013102
43. Csendes T, Garay BM, Bánhelyi B (2006) A verified optimization technique to locate chaotic regions of Hénon systems. J Glob Optim 35:145–160
44. Csendes T, Pál L, Sendín JOH, Banga JR (2008) The GLOBAL optimization method revisited. Optim Lett 2:445–454
45. Geddes CD (2017) Surface plasmon enhanced, coupled and controlled fluorescence. John Wiley & Sons, Inc., Hoboken
46. Maliwal BP, Malicka J, Ignacy G, Gryczynski Z, Lakowicz JR (2003) Fluorescence properties of labeled proteins near silver colloid surfaces. Biopolymers 70:585–594